A Coupled Hydrodynamic–Bottom Boundary Layer Model of Ekman Flow on Stratified Continental Shelves*

TIMOTHY R. KEEN** AND SCOTT M. GLENN

Institute of Marine and Coastal Sciences, Rutgers University, New Brunswick, New Jersey

(Manuscript received 10 June 1993, in final form 10 January 1994)

ABSTRACT

This paper describes a hydrodynamic model with turbulent energy closure that uses a simplified wave–current interaction model of the bottom boundary layer to compute bed drag coefficients. The coupled model is used to investigate the interaction of the upper and lower boundary layers with the geostrophic core flow for simple shelf geometry and forcing, and to evaluate the effects of increased bottom friction on coastal hydrodynamics for summer and winter stratification. The thickness of the bottom boundary layer predicted by the model ranges from 10 to 35 m and is consistent with observations from the California shelf. The increased bottom friction calculated by the coupled model in intermediate water depths increases bottom Ekman veering (leftward in the Northern Hemisphere) by as much as 10° if stratification is strong, thus enhancing downwelling and upwelling. Currents along isobaths in shallow water are uniformly decreased by as much as 25% in the coupled model for both summer and winter initial stratification.

1. Introduction

A useful model for circulation on continental shelves consists of a middepth frictionless geostrophic flow, bounded by surface and bottom boundary layers (Pedlosky 1979), with transport parallel to the wind in the geostrophic layer, to the right of the wind (in the Northern Hemisphere) in the surface layer, and to the left of the wind in the bottom boundary layer. This flow is exemplified by Ekman's elementary current system as it is applied to coastal regions (Neumann and Pierson 1966) and as depicted in Fig. 1a. If a steady wind blows parallel to a Northern Hemisphere coast with land to its right, transport in the upper layer has an onshore component that piles water up along the coast. The resulting pressure gradient drives the geostrophic core and offshore transport in the bottom boundary layer. This flow pattern is called a coastal downwelling regime. If instead the wind blows with the coast to its left, surface transport is offshore and coastal upwelling occurs as bottom water is transported shoreward.

The development of an Ekman current system in coastal regions depends on the thicknesses of the boundary layers, which are in turn functions of stratification and coastal circulation. If the water column is homogeneous, the geostrophic core is modified for water depths less than 2.5 times the thickness of the upper mixed layer (Fig. 1a). When stratification is present the three-layer flow structure depends on the initial stratification and the history of mixing within the boundary layers. The height of the bottom boundary layer is more dependent on water depth than is the upper boundary-layer thickness, because of across-isobath transport of bottom water with different properties, and the effects of decreasing depth on bottom stress and turbulent mixing at the bed. The one-dimensional, time-dependent behavior of the bottom boundary layer in a stratified sea with a sloping bottom has been evaluated using numerical models for both upwelling and downwelling regimes (see Trowbridge and Lentz 1991). These studies demonstrate the dependence of bottom boundary-layer height on both stratification and currents along isobaths.

For water depths above wave base, bottom friction is enhanced by the interaction within the bottom boundary layer of steady currents and the oscillatory currents associated with shoaling wind waves. The time-average interaction of waves and currents within the bottom boundary layer is described by several theories (e.g., Smith 1977; Grant and Madsen 1979; Davies et al. 1988). The model of Grant and Madsen (1979), and a version that includes a suspended sediment stratification correction (Glenn and Grant 1987), have been evaluated for both storm and fair weather conditions by Grant et al. (1984), Cacchione

* Contribution Number 93-37 of the Institute of Marine and Coastal Sciences, Rutgers University.

** Current affiliation: Naval Research Laboratory, Stennis Space Center, Mississippi.

Corresponding author address: Dr. Timothy R. Keen, Naval Research Laboratory, Code 7320, Stennis Space Center, MS 39529.

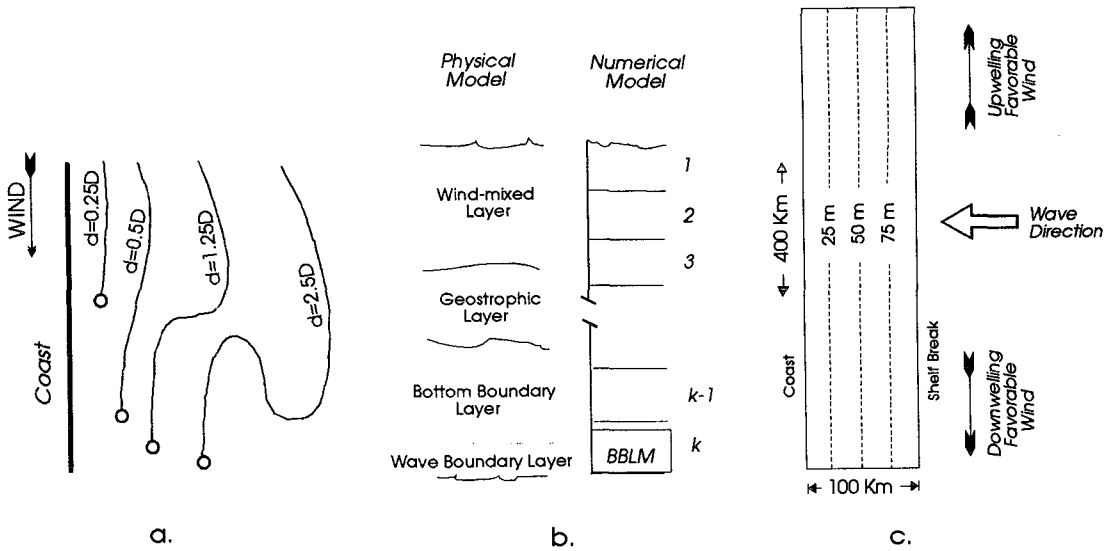

FIG. 1. (a) Current hodographs of the vertical structure of Ekman's elementary current system in a coastal region during a downwelling regime, where d = total water depth and D is the depth of the upper frictional layer. Currents at the surface are marked with an open circle (from Neumann and Pierson 1966). (b) Schematic drawing of the three-layer current system (after Grant and Glenn 1983) and its representation by the model grid. The divisions of the physical model are not to scale in the figure. The numerical model is shown on the right, with lines indicating the numerical model representation of the three-layer current system using k levels of thickness 5 m. The BBLM represents the lowest part of the bottom boundary layer only and includes the wave boundary layer. (c) Plan view of relationships between the model basin, wind stresses, and waves.

et al. (1987), and Drake and Cacchione (1992), and were found to reasonably predict boundary-layer observations from the California shelf.

The Grant and Madsen (1979, henceforth referred to as GM) bottom boundary-layer model (BBLM) has been used in conjunction with hydrodynamic models to evaluate the effects of increased bottom friction on flow for a range of conditions. Spaulding and Isaji (1985) simplified the calculation of the physical bed roughness k_b in the GM model by assuming that bottom velocities are wave dominated and that the bed is rough during a storm. They coupled the simplified BBLM to two- and three-dimensional hydrodynamic models and demonstrated the effects of wave and current bottom friction during storm flows. Analysis of the results for Tropical Storm Delia (Spaulding and Isaji 1987) revealed an overprediction of bottom stresses when the effects of suspended sediment stratification were neglected. Cooper and Thompson (1989) implemented the GM model for Gulf of Mexico hurricanes by first computing drag coefficients for a range of wind stresses, steady currents, and water depths, and then placing them in "lookup" tables. During a model run, the drag coefficient C_d is located within these tables using the parameters at each grid point. The larger bed stresses decreased downwelling and allowed longer integration periods. Signell et al. (1990) developed a simplified model from the GM theory, which calculates C_d for collinear waves and currents. This model was applied to wind-driven circulation in an ideal bay. The results showed that transport rates were significantly modified by the inclusion of wave–current bottom friction and topographic variations become important in shallow depths where waves interact with the bottom. Davies and Lawrence (1993) used the same method as Signell et al. (1990) for tidal- and wind-driven circulation in the eastern Irish Sea, and demonstrated the importance of wave–current interaction in decreasing the magnitudes of currents in shallow water. Davies and Lawrence's (1993) results did not reveal significant changes in current directions caused by increased bottom friction. Keen and Slingerland (1993a,b) used the BBLM of Glenn and Grant (1987) to calculate wave–current bottom shear stresses during tropical cyclones in the western Gulf of Mexico. Although the model system they employed did not couple the BBLM and the hydrodynamic model, their results do show the impact of enhanced bed stresses on sediment entrainment and transport during storms.

The result of this previous work is a general understanding of the evolution of the bottom boundary layer on the continental shelf and the influence of combined wave–current bottom stresses on circulation in shallow seas and estuaries. A reasonable next step in modeling continental shelf sedimentation is to develop a general coupled model for stratified circulation, and to evaluate its behavior for simple geometry and forcing. With this task completed it will be possible to evaluate numerical

hindcasts of historical storms with respect to existing concepts of storm sedimentation as summarized by Duke et al. (1991). The work reported here is, therefore, preliminary to undertaking such hindcasts for the Middle Atlantic Bight of North America.

In an effort to gain a greater understanding of the factors controlling the evolution of flows on stratified shelves, this paper addresses two related questions: 1) How do the upper and lower boundary layers interact with the geostrophic flow and 2) Which hydrodynamic processes can be expected to be enhanced by the interaction of waves and steady currents at the seafloor? To investigate these questions a coupled model has been developed that consists of a hydrodynamic model for computing the flow field and a BBLM to interactively calculate combined wave and current shear stresses. Section 2 presents a modified version of the GM model and describes those components of the hydrodynamic model influenced by incorporating wave–current drag coefficients into its bed shear stress and turbulent energy algorithms. Section 3 compares the numerical results for the uncoupled and coupled model formulations for different stratification and wind regimes for an ideal shelf geometry with two wave fields. Section 4 compares the lower boundary-layer thickness from the model runs to observations and discusses the effects of increased bottom friction on the Ekman current system.

2. The coupled model

a. The wave–current bottom boundary-layer model

The Glenn and Grant (1987, henceforth referred to as GG) BBLM can be used to model the nonlinear wave–current interaction in the bottom boundary layer on the continental shelf. It includes the effects of both suspended sediment stratification on the flow and the variable bottom roughness associated with a moveable bed (Grant and Madsen 1982), which if neglected recovers the original GM solution. Input to the unstratified version for a fixed bottom roughness, as used in this study, includes the maximum wave velocity u_b and excursion amplitude A_b at the top of the wave boundary layer, an observed current speed u_r and direction (relative to the wave) $\bar{\phi}_c$ at a specified height above the bed z_r, and the physical bottom roughness k_b. The current height z_r is assumed to be above the wave boundary layer but within the current logarithmic layer. The wave-enhanced apparent bottom roughness and the time-average shear stress experienced by the current above the wave boundary layer are then computed.

The solution procedure used by GG was developed for accurate applications to a time series of inputs at a single point. When coupled to a three-dimensional hydrodynamic model, however, the BBLM will be applied numerous times at each grid point, so streamlining is required. Simplified schemes for collinear waves and currents have been developed by others for this purpose (e.g., Signell et al. 1990), but in the present application, it is more realistic to assume the waves are traveling toward the shore and the currents are directed nearly along shore. Realizing that the orthogonal limit is probably more important, a time-efficient version of the GG model that includes arbitrary $\bar{\phi}_c$ is formulated to preserve the original form of the model. Details are discussed in the appendix. Furthermore, the GG model has been previously applied to conditions in which waves and currents were of similar magnitude, whereas the version to be coupled to a shelf circulation model must work for the broader range of conditions encountered during a numerical hindcast. The wave-dominated and current-dominated limits of the BBLM are therefore explored in greater detail than previously.

Following GM, the magnitude of the maximum shear stress τ_{cw} is

$$\frac{\tau_{cw}}{\rho} = u_{*cw}^2 = \frac{1}{2} f_{cw} u_b^2 \alpha, \tag{1}$$

where ρ is the water density, u_{*cw} is a friction velocity, f_{cw} is the combined wave and current friction factor, u_b is the maximum wave orbital velocity at the top of the wave boundary layer, and α is a nondimensional function defined as

$$\alpha = 1 + 2\frac{u_a}{u_b}\cos\phi_c + \left(\frac{u_a}{u_b}\right)^2, \tag{2}$$

where u_a and ϕ_c are the unknown current speed and direction (relative to the wave) at a height z_a above the bottom. The magnitude of the time-average shear stress τ_c is

$$\frac{\tau_c}{\rho} = u_{*c}^2 = \frac{1}{2} f_{cw} u_b^2 V_2, \tag{3}$$

where u_{*c}^2 is a friction velocity and V_2 is a nondimensional function used by GM. Here V_2 is derived from the integral over a wave period of the instantaneous bottom shear stress (see GM for details) and is dependent on ϕ_c and the ratio u_a/u_b.

For very small currents relative to waves, GM gives a simplified approximate form for V_2:

$$V_2 = \frac{2}{\pi}\frac{u_a}{u_b}(4 - 3\sin^2\phi_c)^{1/2}, \quad u_a \ll u_b; \tag{4}$$

GG evaluates the complete V_2 integral for larger values of u_a/u_b. To avoid this time-consuming step, the integral was reexamined for large currents relative to waves and was found to approach

$$V_2 = \left(\frac{u_a}{u_b}\right)^2 + \frac{1}{2} - \left(\frac{1}{4} + A\right)\sin^2\phi_c, \quad u_a \gg u_b, \tag{5}$$

where the adjustment factor A is initially assumed to be 0. It is later defined in the appendix. For very large

values of u_a/u_b, the expressions for α (2) and V_2 (5) are dominated by the $(u_a/u_b)^2$ term, and V_2 and α converge as u_a/u_b increases. Substituting into (1) and (3), the maximum and average shear stresses both approach the limit

$$\frac{\tau_{cw}}{\rho} = \frac{\tau_c}{\rho} = \frac{1}{2} f_{cw} u_a^2, \quad u_a \gg u_b. \tag{6}$$

The bottom stresses remain quadratic, but now depend only on the steady current velocity, so the time average is also the maximum. This has an important effect on the wave-enhanced apparent bottom roughness predicted by the combined wave and current theory. Following GM, the apparent bottom roughness k_{bc} is defined as

$$\frac{k_{bc}}{k_b} = \left(30\frac{\delta_w}{k_b}\right)^{(1-u_c^*/u_{cw}^*)} = \left(30\frac{\delta_w}{k_b}\right)^{(1-\sqrt{V_2/\alpha})}, \tag{7}$$

where δ_w is the height of the wave boundary layer equal to $2\kappa u_{*c}/u_{*cw}/\omega$, κ is von Kármán's constant (0.4), and ω is the wave frequency. Examining the limiting values: for small currents $V_2 \to 0$, $\alpha \to 1$, $k_{bc} \to 30\delta_w$, and k_{bc} is independent of k_b; for large currents $V_2/\alpha \to 1$, $k_{bc} \to k_b$, and k_{bc} is independent of waves.

The streamlined version of the BBLM described in the appendix was tested for a broad range of wave and current conditions. For the example discussed here, $u_r = 10$ cm s^{-1}, $\bar{\phi}_c = \pi/2$, $z_r = 250$ cm, and $k_b = 30z_o = 0.1$ cm. For a 10-s surface wave, values of 0.1, 1, 10, 100, and 1000 cm s^{-1} are assigned for the maximum bottom orbital velocity u_b. Although 1000 cm s^{-1} is quite high, waves both 100 times larger and 100 times smaller than the current speed are examined for illustration. The current profiles $u(z)$ are defined by

$$u(z) = \begin{cases} \dfrac{u_{*c}}{\kappa}\dfrac{u_{*c}}{u_{*cw}}\ln\dfrac{z}{z_o}, & z < \delta_w \\ \dfrac{u_{*c}}{\kappa}\ln\left(\dfrac{z}{z_{oc}}\right), & z > \delta_w, \end{cases} \tag{8}$$

where $z_{oc} = k_{bc}/30$. Solid lines plotted in Fig. 2 represent the different current profiles, with the change in slope occurring at the top of the wave boundary layer. The dashed line locates the z intercept of the current above the wave boundary layer z_{oc}, which is related to the apparent bottom roughness length felt by the current. For u_b equal to 10 cm s^{-1}, z_{oc} is an order of magnitude greater than z_o and an order of magnitude less than δ_w. As the wave velocity increases to 100 and 1000 cm s^{-1}, the wave boundary-layer height increases and z_{oc} approaches δ_w. As the wave velocity decreases to 1 and 0.1 cm s^{-1}, the wave boundary-layer height decreases, z_{oc} approaches z_o, and the solution approaches a pure current. The $u_b = 0.1$ cm s^{-1} case is indistinguishable from a pure current line between

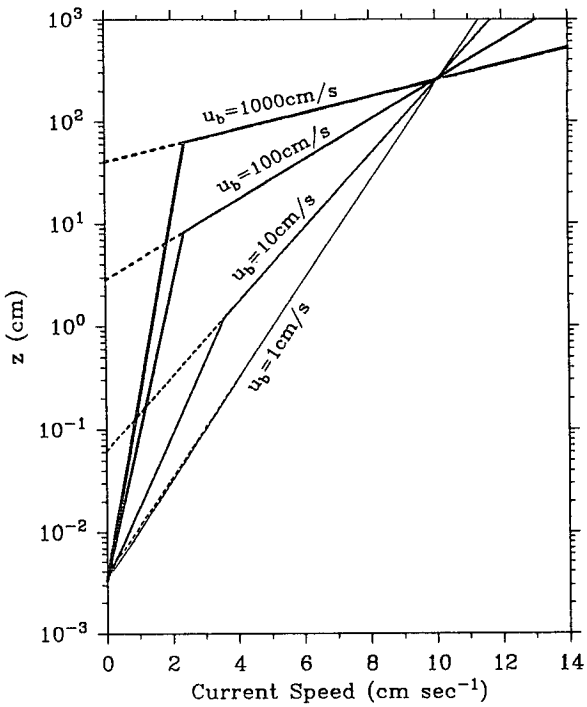

FIG. 2. Model-generated current speed profiles (solid line) for u_b = 1000 cm s^{-1} (δ_w = 62.5 cm), u_b = 100 cm s^{-1} (δ_w = 8.26 cm), u_b = 10 cm s^{-1} (δ_w = 1.21 cm), and u_b = 1 cm s^{-1} (δ_w = 60.47 cm). The location of the z intercept (z_{oc}) for the current above the wave boundary layer is denoted by the dashed line. For this test, u_r = 10 cm s^{-1} at z_r = 250 cm, $\bar{\phi}_c = \pi/2$, and k_{bc} = 0.1 cm.

$u(z_o) = 0$ and $u(z_r) = 10$ cm s^{-1}, and for clarity it is not plotted in Fig. 2.

b. *The hydrodynamic model*

Coastal circulation is calculated using the turbulent energy closure hydrodynamic model of Leendertse and Liu (1978), which solves the primitive equations for turbulent flow as well as conservation equations for salt, heat, and turbulent energy, on an Arakawa C grid comprising model levels stacked to represent water depth (James 1990). As used in this study, the mathematical formulation of the model is presented in Keen and Slingerland (1993a). The bottom shear stress algorithm has been replaced by a quadratic formulation using either a constant value of C_d or one calculated by the BBLM. Their Ekman depth calculation for the thickness of the upper mixed layer is not used because of stratification in the present study. Instead, the wind-mixed layer is represented by the number of upper model levels with similar properties. Resolution is restricted to the thickness of levels used in the hydrodynamic model.

The bottom shear stress for a steady current is given by

$$\tau_b = \rho u_{*c}^2 = \rho C_d |u_r| u_r. \quad (9)$$

Evaluating (8) for u_r at z_r, substituting for u_r in (9), and solving for the drag coefficient gives

$$C_d = \left[\frac{\kappa}{\ln(30z_r/k_{bc})}\right]^2. \quad (10)$$

Since the uncoupled model runs are designed to simulate flow in the absence of waves, k_b and k_{bc} are equivalent and are assigned a value of 0.1 cm, as in the study of Signell et al. (1990). The reference height z_r is the height above the bottom for the computation of currents by the hydrodynamic model, in this case 250 cm. Substituting these values into (10) gives 1.27×10^{-3} for C_d, which is used in all uncoupled numerical experiments.

The vertical exchange of momentum, mass, heat, and turbulence between levels is calculated from an eddy viscosity $A_z = L_o E^{1/2}$, where L_o is a mixing length and E is turbulent kinetic energy. The conservation equation for E contains source terms at the bed, within the water column, and at the surface (Leendertse and Liu 1977). The rate of turbulent energy generation at the bed is calculated from

$$S_b = \frac{a_3 C_d u_r^3}{h}, \quad (11)$$

where a_3 is a constant with a value of 0.08 and h is the thickness of the lowermost model level. The generation term S_b introduces additional turbulence through the greater C_d calculated by the BBLM; consequently, A_z increases vertical mixing, starting at the bed and working upward. Turbulence is generated by shear between model levels from

$$S_e = \frac{1}{2} A_z e^{(-R_2 R_g)} \left[\frac{d\bar{u}}{dz}\right]^2 \bar{h}, \quad (12)$$

where R_2 is a constant equal to 1.4, R_g is the gradient Richardson number, $\bar{u}$ is the rms velocity in the current model level, and $\bar{h}$ is the average thickness of adjacent levels. Turbulence is also introduced at the surface as a boundary condition dependent on wind speed,

$$S_w = \frac{2.8 \times 10^{-9} W^4}{h_1}, \quad (13)$$

where W is the wind speed at 20 m and h_1 is the thickness of the upper model level.

c. *Modeling approach*

When the model is run in the coupled mode, the circulation model calls the BBLM at each grid point and passes the current values of u_r, z_r, u_b, A_b, $\bar{\phi}_c$, and k_b. The BBLM computes the wave–current drag coefficient C_d from (10) and returns this value. The bed shear stress is then calculated by the hydrodynamic model from (9). The experiments discussed here used a constant value of k_b for all water depths. Such a simplification may not be reasonable for all shelves but this work is intended to evaluate the coupled model for conditions such as may be found within the Middle Atlantic Bight, where the bottom is dominated by relict sandy sediment (Knebel 1981).

Incorporating the BBLM within the lowermost model level preserves consistency within the coupled model; vertical exchange within the hydrodynamic model occurs at discrete level interfaces and the continuous eddy viscosity profile calculated by the BBLM would be inconsistent if it were applied across these interfaces. Since the bottom boundary layer is always thicker than 5 m, the outer part of it is represented by the levels in the hydrodynamic model. The BBLM thus acts to increase the vertical resolution within the lowermost level present at a grid point. For the level thicknesses of 5 m used here, the wave boundary layer will be entirely contained within the BBLM because the wave boundary layer is typically from 10 to 30 cm in height. The relationships between the Ekman flow model, the hydrodynamic model, and the BBLM are shown schematically in Fig. 1b.

Deep-water waves approaching a sloping bottom will be refracted so as to approach the coast almost orthogonally, whereas the dominant flow direction of the steady currents is parallel to the coast. Thus, in many situations $\bar{\phi}_c$ can be approximately $\pi/2$ everywhere. The wave–current interaction is significant. For small changes in $\bar{\phi}_c$ near $\pi/2$, the variation of u_{*c} is limited, so $\bar{\phi}_c$ is set equal to $\pi/2$ in all coupled runs as a simple representation of this physical situation. Because the wave crests are assumed to be nearly parallel to isobaths everywhere, refraction will be minor, and shoaling is the only expected modification of incident wave heights. Shoaling, however, changes the height of a 10-s period wave by less than 10% for water depths greater than 10 m, which is the landward limit of the model domain. Therefore, two wave fields with constant wave heights are used. The first wave field is represented by a wave height H of 2 m and a period of 10 s. Bottom orbital parameters for different water depths are found from linear wave theory (Table 1). The second wave field has a wave height of 4 m and the same period, with wave parameters double those from Table 1.

The model runs use a rectangular basin located at 40°N with water depth monotonically increasing from 10 m at the coast to 100 m at the open-sea boundary and represented by 20 levels with a thickness of 5 m each. Twenty grid points of 20-km spacing are used for the north–south axis of the basin. The east–west dimension is 100 km with 20 grid points of 5-km spacing. The resulting bottom slope is 9×10^{-4}. The upper boundary condition consists of a uniform wind stress of 1.5 g cm^{-1} s^{-2} parallel to the coast. Relationships

TABLE 1. Wave parameters for coupled runs with H = 2 m.

	Depth (m)																		
	10	15	20	25	30	35	40	45	50	55	60	65	70	75	80	85	90	95	100
A_b (cm)	136	102	81	66	54	45	37	31	25	21	17	14	12	10	8	6	5	4	4
U_b (cm s^{-1})	86	64	51	41	34	28	23	19	16	13	11	9	7	6	5	4	3	3	2

between the wind forcing, waves, and coastal geometry are shown in Fig. 1c. No flow is allowed perpendicular to the landward boundary and the sea surface height on the open boundary is clamped to 0, with no normal flow. A damped Neuman boundary condition is imposed for water level at the upwind cross-shelf boundary and for horizontal currents, salinity, and temperature at the downwind boundary. These boundary conditions isolate the model region from deep ocean currents, and produce a steady flow parallel to the coast. Stratification extremes occur during summer and winter, and are represented by mean temperature and salinity profiles from the New York Bight for June and February (Bowman 1977), respectively, as initial conditions.

A total of 25 numerical experiments were completed in this study. Many of these were required to determine the combination of boundary conditions and model parameters that produced steady upwelling and downwelling flow fields. This paper discusses only eight (Table 2) for which all model parameters were constant except the wind direction, initial stratification, method of calculating C_d (coupled and uncoupled models), and wave height H. Each run simulates 60 hours using 3600 model integrations (ΔT = 60 s). The uncoupled model requires approximately 130 minutes on a Sun 4/630 MP processor and the coupled model 170 minutes, a 30% increase in cpu time.

3. Comparison of model results

The evolution of the Ekman current system, as well as the effects of increased bed friction, are examined for summer and winter stratification using the 2-m and 4-m wave fields to compute combined wave–current drag coefficients. The model results to be used as a basis for comparison are those from the uncoupled model, which entirely neglects wave effects. An early stage of flow development is demonstrated using model output from hour 12, at which time none of the runs had reached equilibrium, as indicated by momentum balance. Model results for hour 48 are used to illustrate the evolved flow in the following discussion. The upwelling regime is investigated using the uncoupled and coupled models with summer stratification only. The results are summarized in Table 2.

a. Summer stratification

1) DOWNWELLING REGIME WITH H = 2 M

The uncoupled model referred to below is run 16 and the coupled model is run 17 (see Table 2). The results are compared for hours 12 and 48 so as to explain the evolution of several aspects of the flow fields common to all of the model runs to be discussed later. The combined bottom shear stresses above the wave boundary layer u_{*c} oppose the bottom currents calculated by the hydrodynamic model and are, therefore, decomposed into along- and across-isobath components. Since the BBLM reduces to a steady current solution for very small A_b and u_b, the bottom stresses at hour 12 (Fig. 3a) are similar for both models in deeper water. By hour 48 the flow field is fully developed and bed stresses along isobaths (Fig. 3b) are uniform with distance from shore in the uncoupled model, whereas this component decreases steadily offshore in the coupled model. The magnitudes of the across-isobath components, however, are greatest in both models between 45 and 65 km from the coast at hour 48.

Stratification is evaluated in terms of $\sigma_T = (\rho - \rho_0) \times 10^3$, where ρ_0 is the standard density of water (1 g cm^{-3}). The coupled and uncoupled σ_T profiles (Fig. 4a) for stations located at 20, 50, and 80 m are identical at hour 12, with vertical mixing evident only at 20 m. By hour 48 (Fig. 4b), mixing has occurred at all water depths and stratification has been eliminated at 20 m. At 50 and 80 m, the σ_T profile has been modified by mechanical mixing and the introduction of lighter water transported offshore in the bottom boundary layer. Changes in stratification are also dependent on the distribution of turbulent kinetic energy E in addition to advection within the boundary layers. Turbulence in the uncoupled model (Fig. 5a) increases steadily upward for depths less than 50 m at hour 48, and it has contributed significantly to mixing in shallow water. Turbulence is restricted to the upper and lower boundary layers in deeper water, but in the coupled model (Fig. 5b), higher turbulence extends to the surface as far as 60 km offshore.

The characteristic flow field at hour 48 (Fig. 6a) for the uncoupled model reveals large currents along isobaths where turbulence is low (see Fig. 5a) and minimum current speeds in the bottom boundary layer, with a maximum in the upper boundary layer. Flow

TABLE 2. Conditions for numerical experiments and summary of Ekman flow results.

Run	Regime[a]	C_d	Strat.	H[b]	Currents at hour 48[c,d]
16	*D*	0.00127	summer	—	d = 20, total Ekman veering ~15° d = 50, mixed layers overlap at middepth, total Ekman veering ~40° d = 80, geostr core, total Ekman veering ~35°
17	*D*	BBLM	summer	2	d = 20, ~20% decr., <5° offsh. rot. from run 16 d = 50, ~10% decr., <5° offsh. rot. d = 80, geostr. core, <10° offsh. rot. at bot. only
24	*D*	BBLM	summer	4	d = 20, ~23% decr., <5° offsh. rot. from run 16 (bot. only) d = 50, ~10% decr., <5° offsh. rot. at top, ~10° at bot. d = 80, ~18% incr. geostr. curr., ~10° offsh. (bot.)
21	*U*	0.00127	summer	—	d = 20, total Ekman veering ~1° d = 50, thin geostr. core, total Ekman veering ~20° d = 80, thick geostr. core, total Ekman veering ~30°
23	*U*	BBLM	summer	2	d = 20, ~9% incr., total Ekman veering incr. ~10° from run 21 d = 50, ~15° onsh. rot. (bot.), ~5° offsh. rot. (top) d = 80, ~15% incr. (bot.) no rot.
19	*D*	0.00127	winter	—	d = 20, total Ekman veering <1° d = 50, total Ekman veering ~10° d = 80, bound layers overlap, total Ekman veering ~30°
22	*D*	BBLM	winter	2	d = 20, 20% decr., slight incr. in Ekman veering from run 19 d = 50, ~12% decr., total Ekman veering <20° d = 80, no change
25	*D*	BBLM	winter	4	d = 20, ~25% decr., <1° rot. from run 19 d = 50, <5% decr., total Ekman veering <20° d = 80, no change

[a] *D*: downwelling, *U*: upwelling.
[b] H: wave height (m).
[c] d: total water depth (m).
[d] Total Ekman veering is the angle between the surface and bottom currents.

in the upper boundary layer is onshore and decreases in shallow water. Downwelling occurs seaward of 20 m with maximum across-isobath bottom currents located 50 to 70 km from the coast. A geostrophic core can be identified by increased flow along isobaths at middepth where across-isobath currents are negligible. The alongisobath currents calculated by the coupled model (Fig. 6b) are reduced uniformly by more than 5 cm s^{-1} near the coast. This is a 25% reduction for a water depth of 10 m. The differences decrease steadily in a seaward direction until a depth is reached at which the upper and lower boundary layers separate. At that depth the currents in the coupled model are reduced most within the bottom boundary layer.

At hour 12 the currents at 50 and 80 m (Fig. 7a) display three-layer patterns similar to the deep water example from Fig. 1a and bottom Ekman veering increases by less than 5° at all water depths in the coupled model. At hour 48 (Fig. 7b), coupled-model currents are uniformly reduced and reveal weak Ekman veering at 20 m, and at 50 m greater overlap of the upper and lower boundary layers is indicated. A geostrophic core is present at 80 m, but it is closer to the surface than at hour 12, suggesting thickening of the bottom boundary layer between 12 and 48 h.

2) DOWNWELLING REGIME WITH H = 4 M

This section discusses the uncoupled results from run 16 and the coupled results from run 24 (see Table 2) for hour 48 only. The alongisobath bottom shear stresses (Fig. 8) are larger at all depths in the coupled model but the across-isobath components are larger in shallow water only. These shear stresses are also greater than those from the 2-m wave experiment (Fig. 3). The σ_T profiles (Fig. 9) indicate that turbulent mixing has not destroyed the pycnocline at 50 and 80 m, despite the greater bottom stresses. In fact, the density profiles are identical to those from run 17 (coupled model with 2-m waves). The excess turbulence generated through (11) is decreased because of reduced currents at the bottom and is partly balanced by dissipation.

A geostrophic core is recognizable in a cross section (Fig. 10) of the circulation field from the coupled model. This flow is well developed as indicated by the 25 cm s^{-1} contour. Alongisobath currents at the bottom

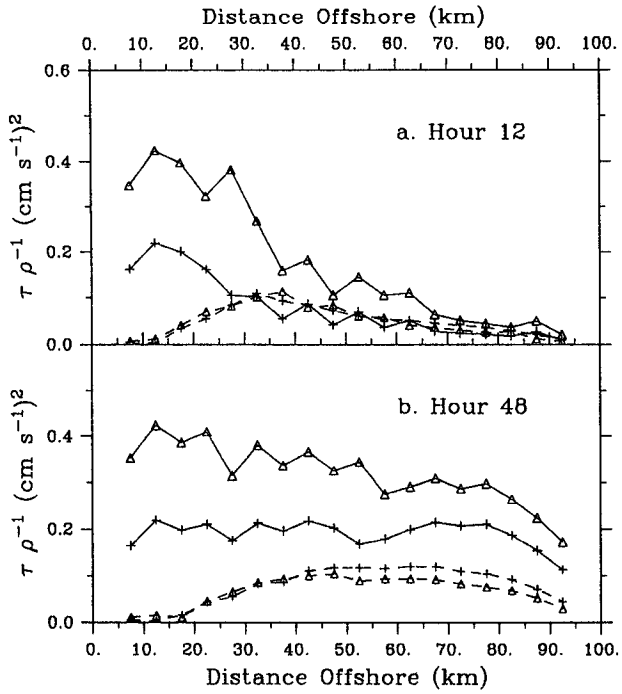

FIG. 3. The downwelling regime with summer stratification and 2-m waves. Distribution of alongisobath (solid line) and across-isobath (dashed line) seafloor shear stress (kinematic) magnitudes for the uncoupled (run 16, crosses) and coupled (run 17, open triangles) models at (a) hour 12 and (b) hour 48.

are smaller than in the uncoupled model (compare to Fig. 6a). The coupled model currents (Fig. 11) at hour 48 are very similar to those from the coupled model with lower waves but they are further reduced at 20 m.

3) UPWELLING REGIME WITH H = 2 M

The model results for hour 48 are discussed in this section. The uncoupled model is run 21 and the coupled model is run 23 (see Table 2). The upwelling regime is simulated using a north-directed wind stress of the same magnitude as in the previous experiments. Stratification (Fig. 12) has been modified at 20 m in both models but a pycnocline persists in the coupled model because of shoreward transport of cold bottom water. Stratification remains at 50 and 80 m as in the downwelling regime. Because of the persistent stratification, the characteristic flow field (Fig. 13a) for the uncoupled model contains strong upwelling in depths as shallow as 40 m, although flow is uniformly along isobaths near the coast. Currents along isobaths are very similar in the coupled model (Fig. 13b) but are slightly higher near the surface on the outer shelf. This result is like that for the downwelling case from Fig. 6b.

Currents at 20, 50, and 80 m (Fig. 14) are consistent with the Ekman current system from Fig. 1a. The angle between surface and bottom currents (total Ekman veering in Table 2) has increased by approximately 10° in the coupled model at 20 m, and by about 20° at 50 m. This increase arises primarily from offshore deflection of surface currents in shallow water, but is partly due to landward rotation of bottom currents at 50 m. Bottom currents are deflected slightly landward at a water depth of 80 m. A three-layer current system persists at 50 and 80 m because of the maintenance of stratification by cold upwelled water, as has been demonstrated elsewhere (Trowbridge and Lentz 1991).

b. Winter stratification

1) DOWNWELLING REGIME WITH H = 2 M

The uncoupled model results discussed below are from run 19 and the coupled results are from run 22 (see Table 2). The comparison focuses on hour 48 except for an analysis of current hodographs that also

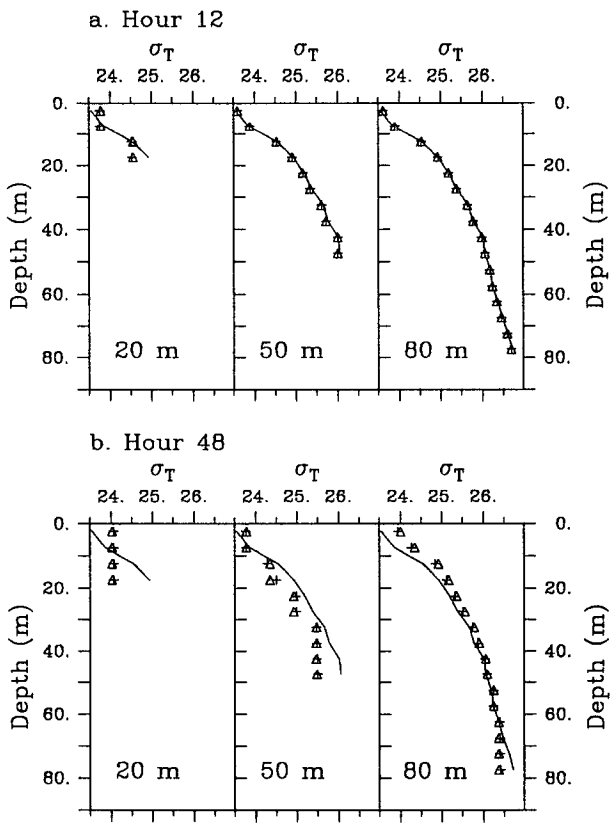

FIG. 4. The downwelling regime with summer stratification and 2-m waves. Profiles of σ_T for a cross section at the center of the basin for water depths 20 m, 50 m, and 80 m at (a) hour 12 and (b) hour 48. The solid line represents the initial distribution, the crosses are the uncoupled model (run 16), and the open triangles are the coupled model (run 17).

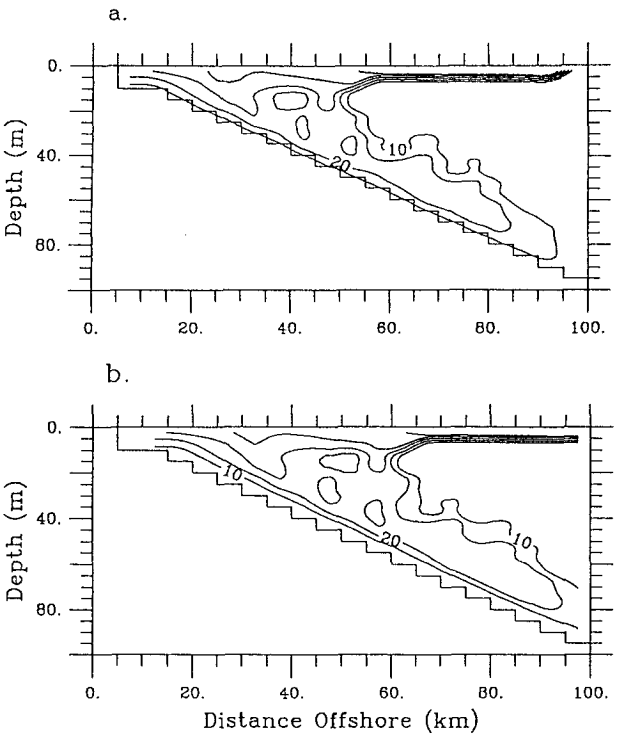

FIG. 5. The downwelling regime with summer stratification and 2-m waves. (a) Cross section perpendicular to the coast of the turbulent kinetic energy density E after 48 h for the uncoupled experiment (run 16). (b) Cross section perpendicular to the coast of E after 48 h for the coupled experiment (run 17). The contour interval is 10 cm^2 s^{-2}.

evaluates hour 12. The initial winter stratification is weak (Fig. 15) and the σ_T profiles for both models at 20 and 50 m are nearly identical at hour 48, whereas at 80 m, a pycnocline is located 45 m below the surface in the uncoupled model, and 35 m below the surface in the coupled model. Here E increases steadily upward (Fig. 16a) in the uncoupled model, because both turbulence generation by shear, and turbulent mixing, are uniformly distributed. Turbulence above the bottom boundary layer (Fig. 16b) is reduced in the coupled model for water depths less than 60 m.

Flow across isobaths (Fig. 17a) is weak landward of 60 m in the uncoupled model, but downwelling occurs within the bottom boundary layer seaward of 60 m. The alongisobath currents calculated by both models increase smoothly from the bed to the surface, but the increased bottom friction in the coupled model has produced weaker flow along isobaths (Fig. 17b) in water depths less than 60 m. Hodographs at hour 12 (Fig. 18a) reveal a geostrophic core in both models at 80 m. Surface currents at 20 m are approximately 10% lower in the coupled model, whereas bottom currents are reduced by approximately 15%. Reductions are less at 50 m but currents near the bed are rotated slightly offshore. At hour 48 (Fig. 18b) neither model predicts a three-layer current system. The current pattern at 20 m is unchanged but the currents at 80 m have evolved and resemble the Ekman current system for $d = 1.25D$ (Fig. 1a).

2) DOWNWELLING REGIME WITH H = 4 M

The uncoupled model compared here is run 19 and the coupled model is run 25 (see Table 2). The discussion is limited to hour 48. The pycnocline at 80 m persists with the larger waves used in the coupled model, and turbulent energy is distributed as in the coupled model with H = 2 m. The differences between the alongisobath currents (Fig. 19) computed by the coupled and uncoupled models are greatest near the bed and decrease upward. Since the currents are not uniformly reduced, it seems that the increased bottom friction associated with the 4-m waves is not being effectively mixed upward, despite the lack of stratification. This may be caused by the limitation of turbulent mixing by the mixing length L_0, which is used to cal-

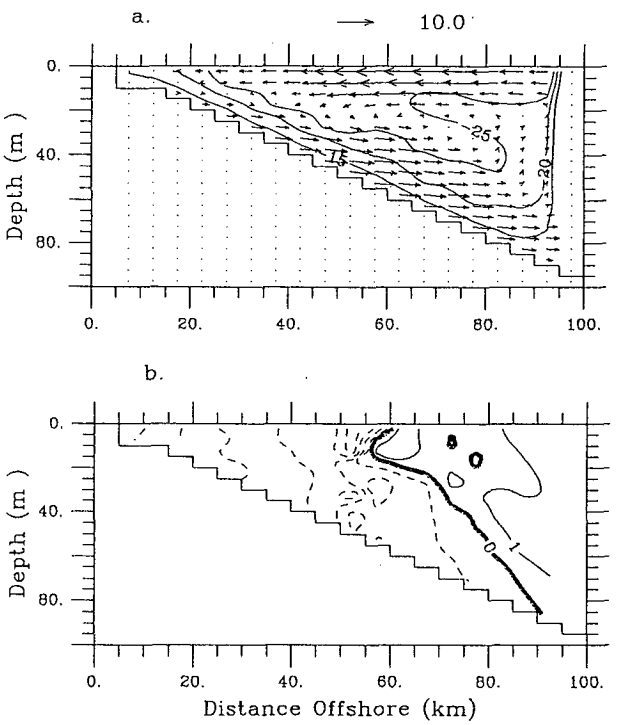

FIG. 6. The downwelling regime with summer stratification and 2-m waves. (a) The flow field for the uncoupled model (run 16) at hour 48. The alongisobath velocity is contoured using an interval of 5 cm s^{-1}, with solid lines for currents out of the page. The vertical velocity component has been multiplied by 100 for clarity. (b) Coupled (run 17) minus uncoupled (run 16) alongisobath current magnitudes at hour 48. Solid contours indicate larger currents out of the page in the coupled model. The contour interval is 1 cm s^{-1}. The wind blows out of the page.

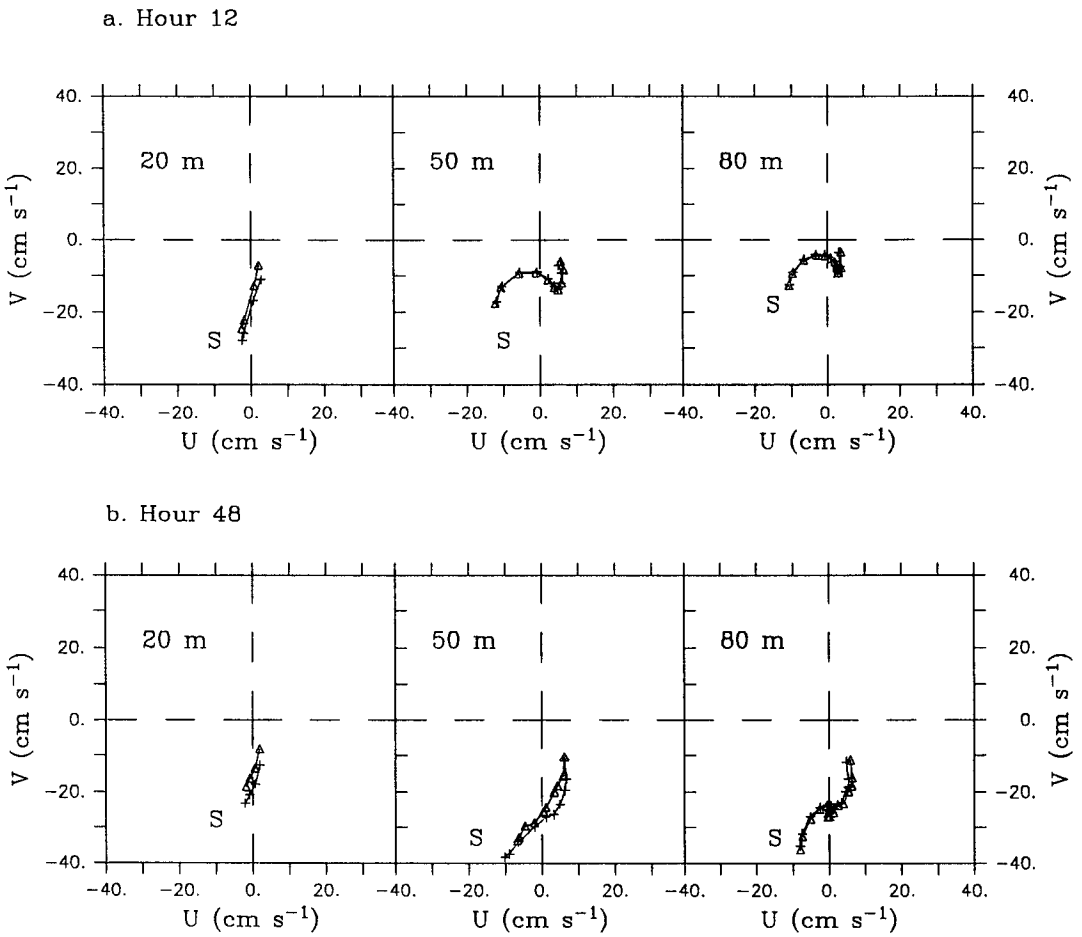

FIG. 7. The downwelling regime with summer stratification and 2-m waves. Hodographs of currents at water depths 20 m, 50 m, and 80 m at (a) hour 12 and (b) hour 48. The uncoupled model (run 16) results are indicated by crosses and the coupled results (run 17) by open triangles. Positive U is east and positive V is north. Surface currents are labeled with an S. The wind blows to the south.

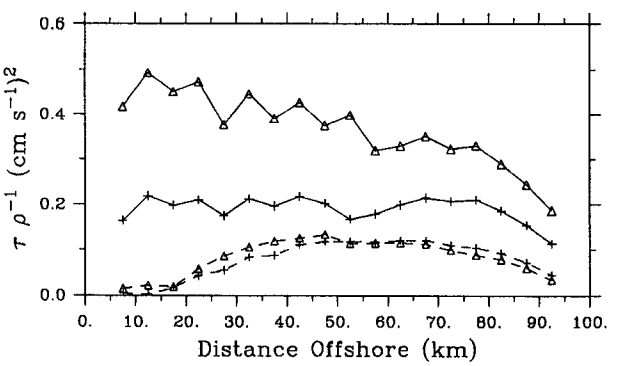

FIG. 8. The downwelling regime with summer stratification and 4-m waves. Distribution of alongisobath (solid line) and across-isobath (dashed line) seafloor shear stress (kinematic) magnitudes for the uncoupled (run 16, crosses) and coupled (run 24, open triangles) models at hour 48.

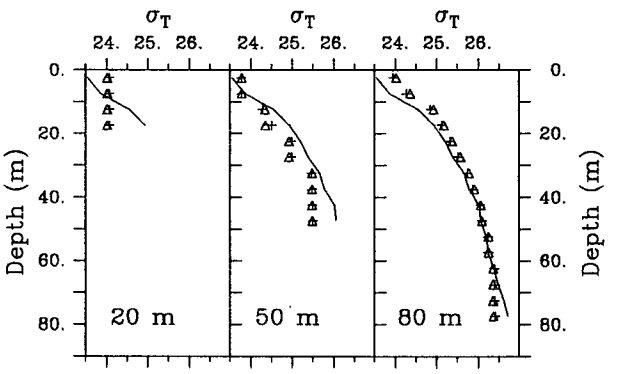

FIG. 9. The downwelling regime with summer stratification and 4-m waves. Profiles of σ_T for a cross section at the center of the basin for water depths 20 m, 50 m, and 80 m at hour 48. The solid line represents the initial distribution, the crosses are the uncoupled model (run 16), and the open triangles are the coupled model (run 24).

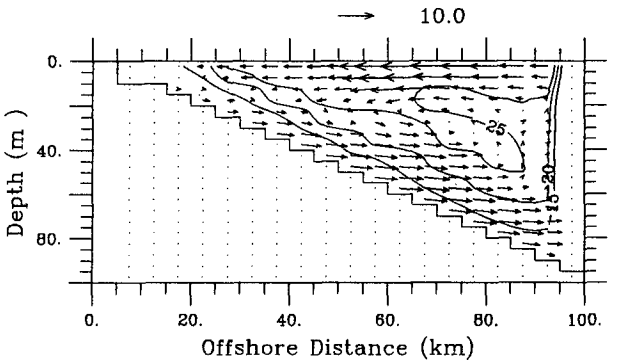

FIG. 10. The downwelling regime with summer stratification and 4-m waves. The flow field for the coupled model (run 24) at hour 48. The alongisobath velocity is contoured using an interval of 5 cm s^{-1}, with solid contours for currents out of the page. The vertical velocity component has been multiplied by 100 for clarity. The wind is blowing out of the page.

culate the vertical eddy viscosity, in addition to turbulence dissipation in the turbulent energy closure scheme. Thus, changes in the currents decrease with time, being constrained by the turbulent transfer of momentum. In fact, the current hodographs at hour 48 (Fig. 20) reveal a vertical structure very like that for 2-m waves but with lower magnitudes at all depths.

4. Discussion

The evolution of an Ekman current system depends on total water depth d relative to the thicknesses of the upper (D) and lower (D^*) boundary layers. In order for a three-layer current system to develop d must be greater than $D + D^*$. For stratified seas the thickness of the boundary layers depends on the eddy viscosity, wind stress, and latitude, as well as the initial density profile. Changes in the density profile occur at the surface and bottom as the upper and lower boundary layers evolve and thicken. Eventually, they can overlap and eliminate the three-layer system.

The following discussion is applicable to shelf- or basin-scale problems for which high resolution in the upper and lower boundary layers is not required. A realistic goal of these studies is to predict the surface water level and the currents at several depths within the water column. The turbulence closure model used in this study incorporates vertical mixing and, if level thicknesses are chosen carefully, the upper part of the lower boundary layer as well as the entire upper boundary layer, can be adequately resolved.

a. *Boundary-layer thickness*

Lentz and Trowbridge (1991) define the lower mixed layer height (herein called D^*) as the maximum height above the bottom at which the temperature is within some range of the temperature at the bottom. In the following discussion D^* is estimated in a similar manner from the distribution of σ_T, E, and alongisobath currents from the model results.

When summer stratification is present in the downwelling experiments, the lower mixed layer, as inferred from the σ_T profile, is 20 m thick for both models at hour 48. The thickness is more difficult to determine from the vertical structure of alongisobath currents but it is in the range of 25 to 35 m. From the distribution of E, however, D^* is 25 m in the uncoupled and 30 m in the coupled model. Analysis of data from CODE-2 reveals a correlation between near-bottom, alongisobath current speed and bottom boundary-layer height (Lentz and Trowbridge 1991). Using a model-calculated current of 18 cm s^{-1} at 7.5 m above the bed (for d = 80 m), the CODE-2 data suggest a height of approximately 20 m for a downwelling regime. This is in excellent agreement with the model results for the

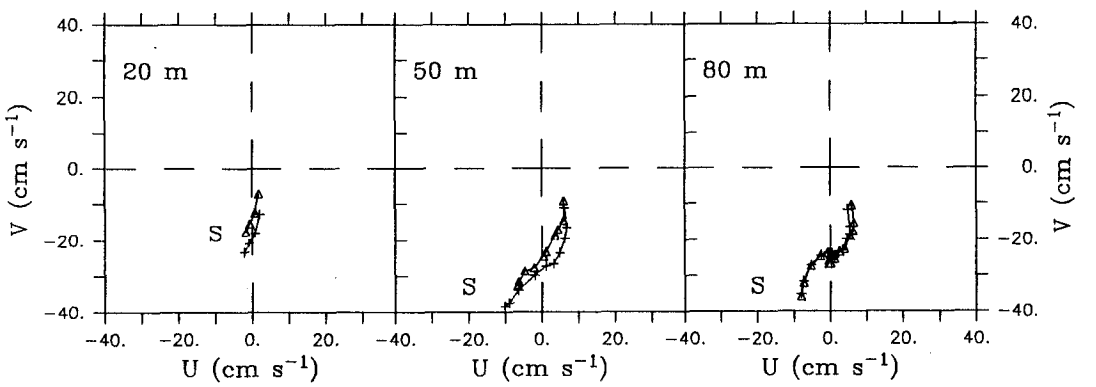

FIG. 11. The downwelling regime with summer stratification and 4-m waves. Hodographs of currents for water depths 20 m, 50 m, and 80 m at hour 48. The uncoupled model (run 16) results are indicated by crosses and the coupled results (run 24) by open triangles. Positive U is east and positive V is north. Surface currents are labeled with an S. The wind blows to the south.

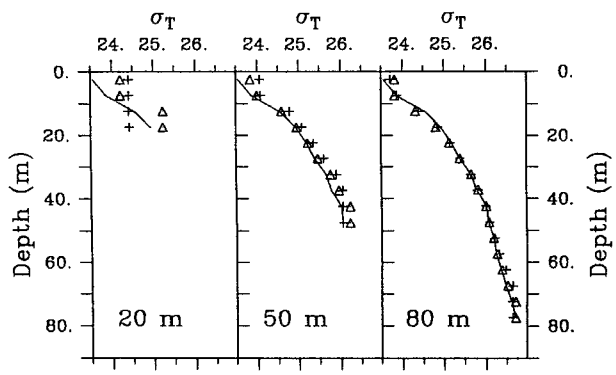

FIG. 12. The upwelling regime with summer stratification and 2-m waves. Profiles of σ_T for a cross section at the center of the basin for water depths 20 m, 50 m, and 80 m at hour 48. The solid line represents the initial distribution, the crosses are the uncoupled model (run 21), and the open triangles are the coupled model (run 23).

thickness inferred from the density profile, and it is consistent with the current- and turbulence-based estimates.

The upwelling model results for the height of the bottom mixed layer are different for the coupled and uncoupled models. Estimating D^* from σ_T gives values of 10 and 15 m for the coupled and uncoupled models, respectively, at 80 m. The thickness inferred from density and momentum distributions are 10 and 15–20 m, respectively, in the uncoupled model. The CODE-2 data suggest a value of 5–10 m for an alongisobath current speed of 10 cm s^{-1}, as taken from the model results. Based on the variability of the observations, and differences in stratification between the model and the California shelf, the discrepancies are thought to be acceptable. This is encouraging since the model equations do not include a bottom slope term that would contribute to reducing the height of the bottom boundary layer.

The upper boundary layer, as identified by the σ_T profiles, is initially 10 m thick for summer stratification, but at hour 48, there is no distinctive pycnocline in deep water. Instead, the density gradient decreases smoothly in the upper water column. As inferred from the currents in the cross sections, however, D would appear to be approximately 20 m for all model results.

Boundary-layer thickening in the model does not continue uninhibited for realistic situations because of feedback in the turbulent energy computations. As currents within the boundary layer become more uniform, turbulent energy production by current shear is reduced and dissipation rates, which are a function of E, come to equilibrium with production. Although the density profile will become vertically uniform, given enough time, the rate of mixing slows appreciably as indicated by models of the bottom boundary layer (see Trowbridge and Lentz 1991).

b. *Evolution of Ekman flow*

The increased bed drag calculated by the BBLM will eventually decrease currents throughout the water column through momentum exchange if stratification is weak, as in shallow depths for all of the downwelling experiments. Increased turbulence generation at the bed by (11) improves vertical exchange of not only momentum, but also heat, salt, and turbulence through the vertical eddy viscosity. Vertical mixing is also enhanced by turbulence generated by shear between model levels through (12). A balance between turbulence generation and vertical mixing and dissipation was maintained near the bed, resulting in lower magnitudes of turbulent energy at the bed in the coupled model but with increased turbulence within the water column (see Figs. 5 and 16). As the density profile near the bottom is modified by this mixing, the bottom boundary layer progressively thickens and erodes the geostrophic core. The upper boundary layer is insensitive to increased bottom friction and thickens with time in response to the constant wind stress.

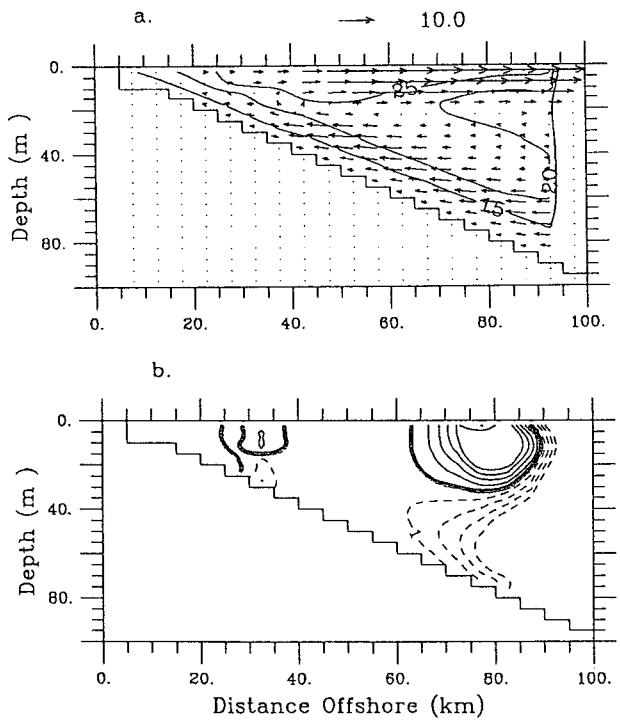

FIG. 13. The upwelling regime with summer stratification and 2-m waves. (a) Flow field at hour 48 for the uncoupled model (run 21). The alongisobath velocity is contoured using an interval of 5 cm s^{-1}. Solid contour lines indicate currents into the page. The vertical velocity component has been multiplied by 100 for clarity. (b) Coupled (run 23) minus uncoupled (run 21) alongisobath current magnitudes at hour 48. Solid contours indicate larger currents into the page in the coupled model. The contour interval is 1 cm s^{-1}. The wind blows into the page.

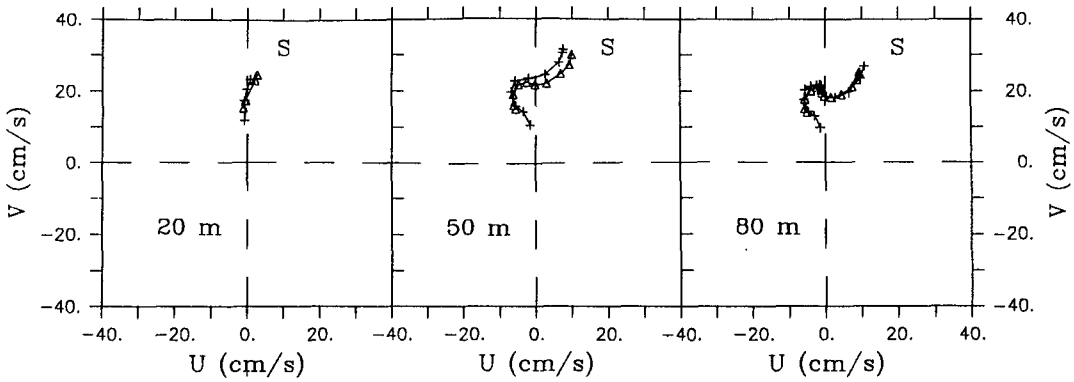

FIG. 14. The upwelling regime with summer stratification and 2-m waves. Hodographs of currents for water depths 20 m, 50 m, and 80 m at hour 48. The uncoupled (run 21) results are indicated by crosses and the coupled results (run 23) by open triangles. Positive U is east and positive V is north. Surface currents are labeled with an S. The wind blows to the north.

After 12 h in the downwelling experiments with summer stratification, the upper and lower boundary layers do not overlap at a water depth d of 50 m, and the current system (Fig. 7a) is similar to that for $d = 2.5D$ from Fig. 1a. Using $D = 20$ m, as estimated from the σ_T profile, the model result is consistent with the ideal current system. As expected, there is no change in this structure in going to deeper water. By hour 48, turbulence (and hence A_z) in the model is high throughout the water column at 50 m and the hodograph (Fig. 7b) reveals a current structure like that for $d = 0.5D$. At 80 m the turbulent energy distribution is similar to the eddy viscosity profile used in Ekman's elementary current system (Neumann and Pierson 1966), and the resulting currents resemble those for $d = 2.5D$.

The bottom boundary-layer height in the experiments with summer stratification is smaller during upwelling than downwelling, in agreement with the observations of Lentz and Trowbridge (1991). Thus, at hour 48 the upwelling current system at 50 m (Fig. 14) is the same as for $d = 1.25D$, while the deep-water pattern is present at 80 m. The persistent pycnocline at 20 m allows a current pattern appropriate to d

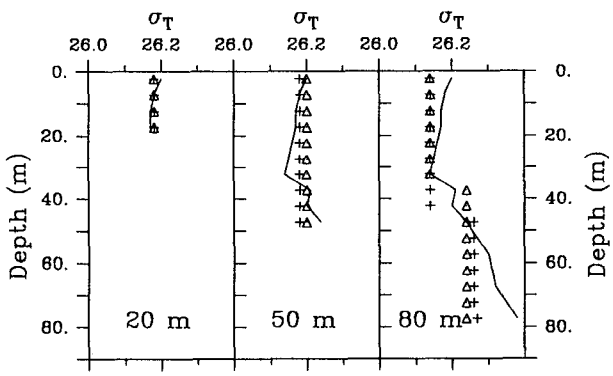

FIG. 15. The downwelling regime with winter stratification and 2-m waves. Profiles of σ_T for a cross section at the center of the basin for water depths 20 m, 50 m, and 80 m at hour 48. The solid line represents the initial distribution, the crosses are the uncoupled model (run 19), and the open triangles are the coupled model (run 22).

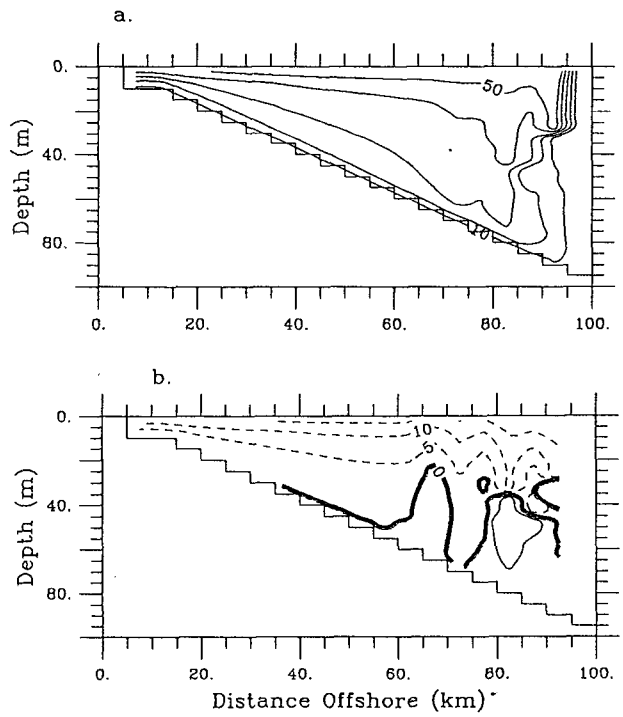

FIG. 16. The downwelling regime with winter stratification and 2-m waves. (a) Cross-shelf distribution of turbulent kinetic energy density E for the uncoupled model (run 19) at hour 48. The contour interval is 10 cm^2 s^{-2}. (b) Coupled (run 22) minus uncoupled (run 19) E at hour 48. Solid contours indicate greater turbulence in the coupled model. The contour interval is 5 cm^2 s^{-2}.

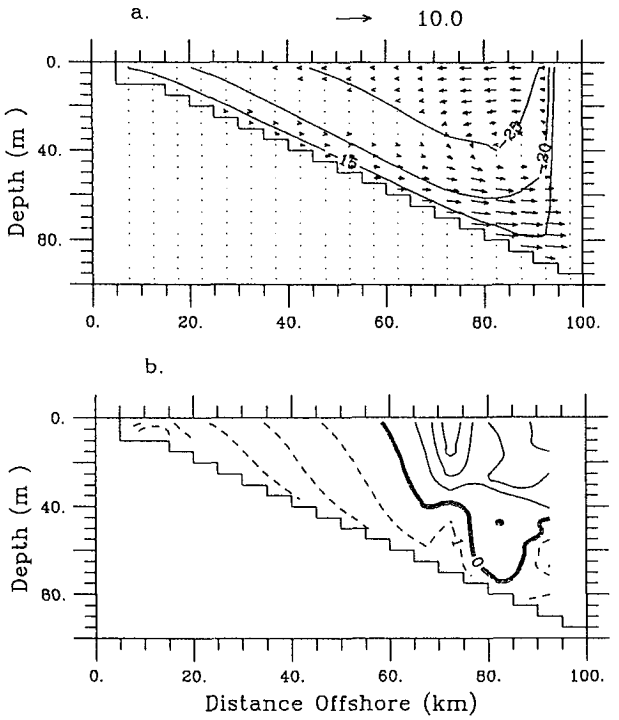

FIG. 17. The downwelling regime with winter stratification and 2-m waves. (a) Flow field at hour 48 for the uncoupled model (run 19). The alongisobath velocity is contoured using an interval of 5 cm s^{-1}, and solid contours indicate flow out of the page. The vertical velocity component has been multiplied by 100 for clarity. (b) Coupled (run 22) minus uncoupled (run 19) alongisobath current magnitudes at hour 48. Solid contours indicate larger currents out of the page in the coupled model. The contour interval is 1 cm s^{-1}. The wind blows out of the page.

$= 0.5D$ to develop in the coupled model, instead of $d = 0.25D$.

The primary result of increasing drag coefficients when stratification is weak is to decrease currents at all depths, with weak Ekman veering near the bed. From experiments with winter stratification, between hours 12 and 48 the currents in deeper water evolved toward the shallow water limit. There was no change at 20 m and very little at 50 m. The currents at 80 m resembled the Ekman system for $d = 1.25D$ at hour 12, but by hour 48 they are like that for $d = 0.5D$.

5. Summary and conclusions

This paper introduces a coupled model for application to circulation in stratified coastal seas. The hydrodynamic model includes a turbulent energy closure scheme and vertical mixing of momentum, heat, mass, and turbulence. A time-efficient version of the Grant and Madsen (1979) wave–current bottom boundary-layer model is used to calculate bottom drag coefficients for use in the hydrodynamic model. By implicitly including the surface and bottom boundary layers the model is able to simulate the development of Ekman's elementary current system in coastal regions (Neumann and Pierson 1966), and the results have been presented for a transect across isobaths at the center of a rectangular basin with a bottom gradient of 9×10^{-4}.

This study set out to identify interactions between the upper and lower boundary layers and the geostrophic core for Ekman's elementary current system, which are affected by increasing bottom friction because of combined wave–current drag coefficients. Changes in Ekman flow predicted by these numerical experiments are summarized in Table 2, and several statements can be made concerning the questions stated in the introduction.

1) The thickness of the bottom boundary layer calculated by the model for both upwelling and downwelling regimes is consistent with observations from the California coast for similar water depths (Lentz and Trowbridge 1991). The predicted heights are 20–35 m for downwelling and 10–20 m for upwelling.

2) The model-calculated coastal current system is similar to Ekman's elementary current system, with the depths at which different current structures are predicted to occur in the model differing from Ekman's theory because of stratification and variable eddy viscosity profiles. The elementary current system is a first-order approximation to coastal flows, which the model is able to improve by allowing the boundary layers to evolve.

3) With increasing wind duration the upper and lower boundary layers thicken and overlap in shallow water, causing the geostrophic core to migrate offshore. After 48 h, a three-layer current system is located at a water depth of 65 m when strong stratification is present during an upwelling event, and at a depth of 80 m during downwelling. It is absent when stratification is weak.

4) Turbulent kinetic energy near the bed is lower in the coupled models because the wave–current drag coefficients reduce bottom currents sufficiently to decrease turbulence generation, which is dependent on u_r^3. However, turbulence above the bed is increased by greater current shear and enhanced vertical mixing, resulting in thickening of the bottom boundary layer.

5) When stratification persists, as in the summer upwelling experiment, Ekman veering within the bottom boundary layer is increased at all water depths. This additional rotation enhances both upwelling and downwelling.

6) The currents calculated in shallow water (less than 30 m) are as much as 25% less in the coupled model. This disparity decreases offshore. Because of effective vertical mixing at shallow depths there is little difference between strong and weak stratification.

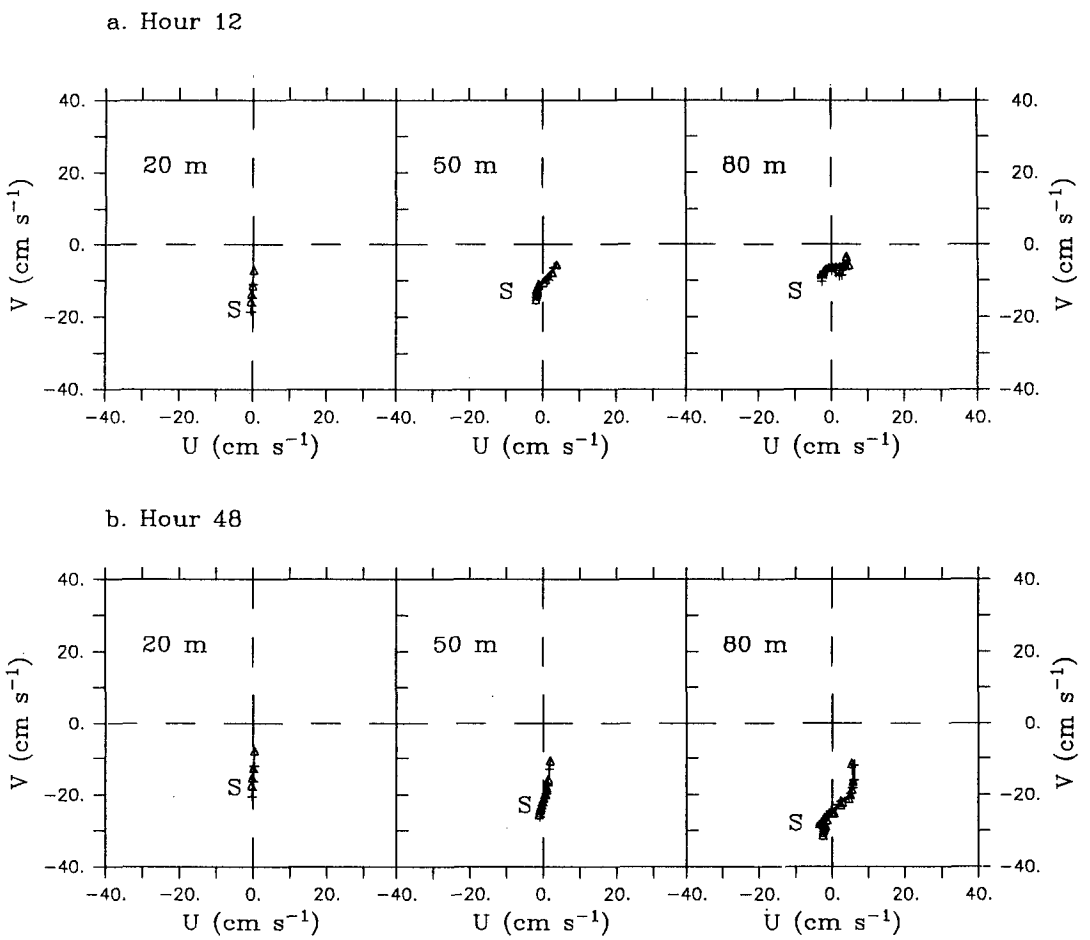

FIG. 18. The downwelling regime with winter stratification and 2-m waves. Hodographs of currents for water depths 20 m, 50 m, and 80 m at (a) hour 12 and (b) hour 48. The uncoupled model results (run 19) are indicated by crosses and the coupled results (run 22) by open triangles. Positive U is east and positive V is north. Surface currents are indicated by S. The wind blows to the south.

7) The variability of currents associated with wave–current bottom stresses in stratified seas cannot be simply described, because nonlinear interaction between the boundary layers and the geostrophic core, and turbulent mixing within the boundary layers, produce complex responses, even for simple bathymetry and forcing.

These results show that the general coupled model presented in this paper reasonably predicts several important processes and interactions that occur in stratified coastal seas. They further demonstrate the importance of wave–current interaction for evolving Ekman flows in coastal regions. The coupled model addresses several problems related to sedimentation on continental shelves discussed by Keen and Slingerland (1993a), such as spatially variable and evolving stratification during storms and the inclusion of wave–current bottom stresses in the hydrodynamic calculations. It can also be used to evaluate the applicability of the storm sedimentation model most frequently used by earth scientists (Duke et al. 1991). Although it is first necessary to evaluate the model's predictions under more difficult conditions for which verification data are available, it is feasible to apply the coupled model to more realistic shelf geometries using hindcast winds and waves in order to evaluate circulation and sedimentation patterns during strong forcing events such as tropical and extratropical cyclones. By using a model that directly incorporates more physical processes, new insight can be gained into the question of sediment transport processes and paths, and the textural evolution of continental shelf sediments.

Acknowledgments. This work was completed while the first author was a Postdoctoral Fellow at the Institute of Marine and Coastal Sciences. The second author was partially supported by funds from the NOAA/

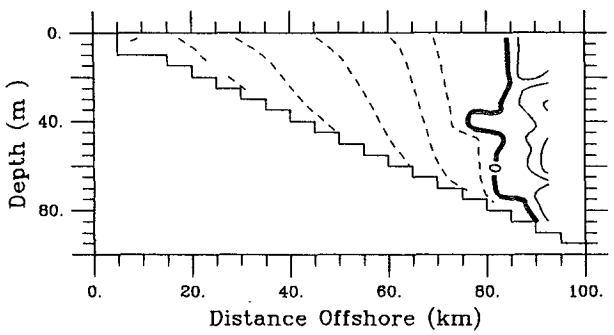

FIG. 19. The downwelling regime with winter stratification and 4-m waves. Coupled (run 25) minus uncoupled (run 19) alongisobath current magnitudes at hour 48. The contour interval is 1 cm s^{-1}. Solid contours indicate larger currents out of the page in the coupled model. The wind blows out of the page.

NURP New York Bight Center. Contribution Number 93-37 of the Institute of Marine and Coastal Sciences, Rutgers University.

APPENDIX

BBLM Modifications

The most computationally intensive sections of the original GG BBLM are (a) calculation of the time-average shear stress; (b) solution of the combined wave and current friction factor equation; and (c) iterating to find the proper current velocity to use in calculating the friction factor and time-average shear stress. The BBLM was modified as discussed below to reduce run time.

a. Time-average shear stress

Equations (4) and (5) for V_2 are compared to the full V_2 integral in Fig. A1 for collinear ($\phi_c = 0$) and orthogonal ($\phi_c = \pi/2$) waves and currents. The small current approximation (4) is applicable for values of u_a/u_b as large as 0.4 for the collinear case or 0.2 for the orthogonal case. The large current expression (5) is a good approximation to the V_2 integral for values of u_a/u_b as low as 0.8 for collinear waves and currents. Comparisons for other values of ϕ_c showed that the greatest discrepancy between (5) and the V_2 integral occurs when waves and currents are perpendicular, in which case (5) does not work as well for values of u/u_b below 1 (Fig. A1b). The difference between (5) and the V_2 integral increases exponentially as u_a/u_b decreases. A convenient functional form for the adjustment factor A in (5) that eliminates much of the exponential difference is

$$A = 0.43 \exp\left[-1.2\left(\frac{u_a}{u_b} - 0.85\right)\right]. \quad \text{(A1)}$$

Substituting (A1) into (5) gives the adjusted large current result shown in Fig. A1b, and it is good for values of u_a/u_b as low as 0.6. The adjustment factor A is modulated by the $\sin^2\phi_c$ term in (5) and so does not affect the collinear case.

For collinear waves and currents (Fig. A1a) the V_2 integral is not closely approximated by either small or large current approximations when the value of u_a/u_b is between 0.4 and 0.8. For orthogonal waves and currents (Fig. A1b), neither the small current nor adjusted large current approximations are valid for values of u/u_b between 0.2 and 0.6. Furthermore, it was found that the 0.4-unit range of u_a/u_b for which neither approximation was valid varied almost linearly with ϕ_c between 0 and $\pi/2$. Rather than evaluate the complete V_2 integral for this intermediate range of u_a/u_b, a linear interpolation between the large and small current limits was found to match the integral well; therefore, a ϕ_c-dependent intermediate range of u_a/u_b is defined. Equation (4) is used to find V_2 when u_a/u_b is less than

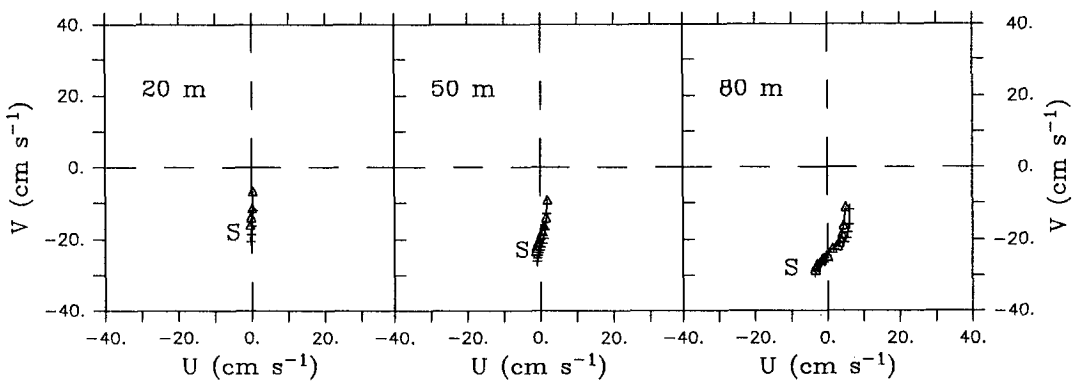

FIG. 20. The downwelling regime with winter stratification and 4-m waves. Current hodographs for water depths 20 m, 50 m, and 80 m at hour 48. The uncoupled model results (run 19) are indicated by crosses and the coupled results (run 25) by open triangles. Positive U is east and positive V is north. Surface currents are labeled by S. The wind blows to the south.

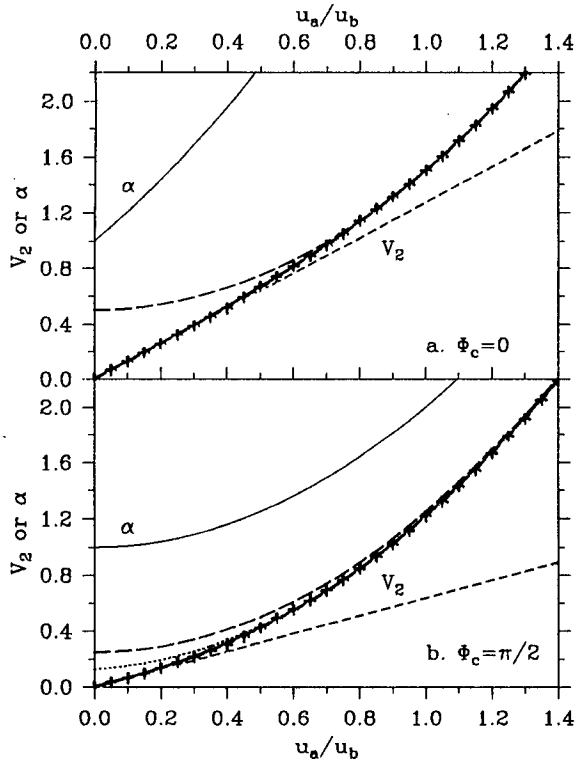

FIG. A1. Plot of V_2 and α as a function of u_a/u_b for (a) $\phi_c = 0$ and (b) $\phi_c = \pi/2$. Key: α, thin solid line; integral solution for V_2, heavy solid line; small current approximation for V_2, small dashed line; large current approximation for V_2, large dashed line; adjusted large current approximation for V_2, dotted line; model approximation to V_2, crosses.

the value of $0.4-0.2[\phi_c/(\pi/2)]$, while (5) is used with the function A given by (A1) when u_a/u_b exceeds $0.8-0.2[\phi_c/(\pi/2)]$. Here V_2 is obtained by linear interpolation between these limits for intermediate values of u_a/u_b. Results using this approximation (plotted as crosses in Fig. A1) differ by less than a few percent from the full integral for V_2. This error is considered acceptable because the approximate version used here is nearly 30 times faster than evaluating the integral.

b. *Wave-current friction factor*

The expression for f_{cw} in GM is a complicated function of u_a/u_b, ϕ_c, and the relative roughness k_b/A_b, where A_b is the excursion amplitude of the wave at the top of the wave boundary layer. Any attempt to approximate the friction factor equation with simple functions is hampered by its dependence on these three variables. Grant and Glenn solved the expression for f_{cw} iteratively by the Newton–Raphson method, which requires two initial guesses for the solution before this rapidly convergent technique can be applied. The number of iterations required to find f_{cw} has been reduced by using simple functions to generate the initial guesses.

The wave-current friction factor f_{cw} can vary over several orders of magnitude, with most variability caused by orders of magnitude variation in the relative roughness, whereas much less variation is due to u_a/u_b or ϕ_c. Therefore, the value of the friction factor in the pure wave limit f_w is estimated first, and since it is a function of k_b/A_b only, it can be approximated by a power law of the form $f_w = B(k_b/A_b)^c$. The parameters B and c have been determined for each decadal variation in k_b/A_b (Table A1). To account for decreasing f_{cw} with increasing u_a/u_b, the pure wave friction factor is adjusted to obtain a first guess:

$$f_{cw1} = \begin{cases} f_w, & u_a/u_b < 0.2 \\ f_w/(1 + (u_a/u_b - 0.2)/1.9), & \\ & 0.2 < u_a/u_b < 4.0 \\ f_w/(1 + \sqrt{u_a/u_b}), & 4.0 < u_a/u_b. \end{cases} \quad \text{(A2)}$$

This approximation is a good upper limit on f_{cw} for values of u_a/u_b less than 4. A lower limit for u_a/u_b less than 4 that makes a convenient second guess is

$$f_{cw2} = f_w/[1 + (u_a/u_b)^{1.2}], \quad u_a/u_b < 4.0. \quad \text{(A3)}$$

For larger currents the second guess is found by halving or doubling the first guess, depending on whether it is too large or too small, respectively. Using the initial guesses from (A2) and (A3), and a tolerance of a few percent of the true value, improves convergence from typically 5–15 iterations to about 1–5.

c. *Iteration to find u_a/u_b*

The third time sink in the GG model is the procedure to find a value of u_a/u_b, such that u_{*c} and $z_{oc} = k_{bc}/30$ satisfy

$$u_r = \frac{u_{*c}}{\kappa} \ln\left(\frac{z_r}{z_{oc}}\right). \quad \text{(A4)}$$

Execution time is again reduced by improving the two initial guesses for u_a/u_b used in the Newton–Raphson solution. A good first approximation of u_a/u_b for arbitrary currents is

TABLE A1. Pure wave friction factor approximation.

k_b/A_b	B	c
$1.0-10^{-1}$	0.2361730	0.617881
$10^{-1}-10^{-2}$	0.1588940	0.445759
$10^{-2}-10^{-3}$	0.0927407	0.328840
$10^{-3}-10^{-4}$	0.0549209	0.252996
$10^{-5}-10^{-6}$	0.0345843	0.202781
$10^{-6}-0.0$	0.0231884	0.168060

$$u_a/u_b = \begin{cases} u_r/u_b, & u_r/u_b > 1 \\ (u_r/u_b)^2, & u_r/u_b < 1. \end{cases} \quad \text{(A5)}$$

If the first guess is too small or too large it is doubled or divided by 10, respectively, to find the second guess. Using (A5) to find the two initial guesses, and stopping the iterations once the solution is found within a few percent, convergence typically occurs in 1–3 iterations instead of 4–20.

REFERENCES

Bowman, M. J., 1977: *Hydrographic Properties. MESA New York Bight Atlas Monograph,* No. 1, New York Sea Grant Institute.

Cacchione, D. A., W. D. Grant, D. E. Drake, and S. M. Glenn, 1987: Storm-dominated bottom boundary layer dynamics on the northern California continental shelf: Measurements and predictions. *J. Geophys. Res.,* **92,** 1817–1827.

Cooper, C., and J. D. Thompson, 1989: Hurricane-generated currents on the outer continental shelf. 1: Model formulation and verification. *J. Geophys. Res.,* **94,** 12 513–12 539.

Davies, A. M., and J. Lawrence, 1993: Examining the influence of wind and wind-wave turbulence on tidal currents, using a 3D hydrodynamic model including wave-current interaction. *J. Phys. Oceanogr.,* in press.

——, R. L. Soulsby, and H. L. King, 1988: A numerical model of the combined wave and current bottom boundary layer. *J. Geophys. Res.,* **93,** 491–508.

Drake, D. E., and D. A. Cacchione, 1992: Wave-current interaction in the bottom boundary layer during storm and non-storm conditions: Observations and model predictions. *Contin. Shelf Res.,* **12,** 1331–1352.

Duke, W. L., R. W. Arnott, and R. J. Cheel, 1991: Shelf sandstones and hummocky cross-stratification: New insights on a stormy debate. *Geology,* **19,** 625–628.

Glenn, S. M., and W. D. Grant, 1987: A suspended sediment stratification correction for combined wave and current flows. *J. Geophys. Res.,* **92,** 8244–8264.

Grant, W. D., and O. S. Madsen, 1979: Combined wave and current interaction with a rough bottom. *J. Geophys. Res.,* **84,** 1797–1808.

——, and ——, 1982: Moveable bed roughness in unsteady oscillatory flow. *J. Geophys. Res.,* **87,** 469–481.

——, and S. M. Glenn, 1983: Continental shelf bottom boundary layer model. Vol. 1, Theoretical model development. Final Rep. to Pipeline Res. Comm., Project PR-153-126, Amer. Gas Assoc.

——, A. J. Williams, and S. M. Glenn, 1984: Bottom stress estimates and their prediction on northern California continental shelf during CODE-1: The importance of wave–current interaction. *J. Phys. Oceanogr.,* **14,** 506–527.

James, I. D., 1990: *Modeling Marine Systems.* CRC Press, 345–372.

Keen, T. R., and R. L. Slingerland, 1993a: A numerical study of sediment transport and event bed genesis during Tropical Storm Delia. *J. Geophys. Res.,* **98,** 4775–4791.

——, and ——, 1993b: Four storm-event beds and the tropical cyclones that produced them: A numerical hindcast. *J. Sed. Petrol.,* **63,** 218–232.

Knebel, H. J., 1981: Processes controlling the characteristics of the surficial sand sheet, U.S. Atlantic outer continental shelf. *Mar. Geol.,* **42,** 349–368.

Leendertse, J. J., and S. K. Liu, 1977: A three-dimensional model for estuaries and coastal seas. Vol. 4, Turbulent energy computation. Report R-2187-OWRT, Rand Corp.

——, and ——, 1978: *Hydrodynamics of Estuaries and Fjords.* Elsevier, 387–405.

Lentz, S. J., and J. H. Trowbridge, 1991: The bottom boundary layer over the northern California shelf. *J. Phys. Oceanogr.,* **21,** 1186–1201.

Neumann, G., and W. J. Pierson Jr., 1966: *Principles of Physical Oceanography.* Prentice-Hall, 545 pp.

Pedlosky, J., 1979: *Geophysical Fluid Dynamics.* Springer-Verlag, 624 pp.

Signell, R. P., R. C. Beardsley, H. C. Graber, and A. Capotondi, 1990: Effect of wave-current interaction on wind-driven circulation in narrow, shallow embayments. *J. Geophys. Res.,* **95,** 9671–9678.

Smith, J. D., 1977: *The Sea.* Vol. 6. Wiley-Interscience, 539–577.

Spaulding, M. L., and T. Isaji, 1985: Design flow conditions near bottom, phase II, coupling of a continental shelf hydrodynamics model to a bottom boundary layer model. Vol. 1, Theoretical development and application. Final Rep. to Pipeline Res. Comm., Project PR-169-1186, Amer. Gas Assoc.

——, and ——, 1987: *Three Dimensional Models of Marine and Estuarine Dynamics.* Elsevier, 405–426.

Trowbridge, J. H., and S. J. Lentz, 1991: Asymmetric behavior of an oceanic boundary layer above a sloping bottom. *J. Phys. Oceanogr.,* **21,** 1171–1185.